JOURNAL OF AIRCRAFT
Vol. 40, No. 2, March–April 2003

Method for Designing Leading-Edge Fillets to Eliminate Flow Separation

Bradford E. Green* and John L. Whitesides†
The George Washington University at NASA Langley Research Center, Hampton, Virginia 23681

A design method is presented whereby the flow separation in the wing–fuselage juncture of aircraft is eliminated by the use of a leading-edge fillet. The design method uses a design rule that relates a change in skin friction to a change in surface slope. After determining the current skin-friction distribution on the plate ahead of the leading edge of the wing, a target skin-friction distribution that will eliminate flow separation is calculated. By the use of the design rule, the current skin-friction distribution is moved toward the target distribution by extending the leading edge of the wing to form a leading-edge fillet. The new leading-edge fillet is then analyzed by the flow solver and the process is iterated until convergence is achieved.

Nomenclature

A	=	proportionality constant in design rule
C_D	=	drag coefficient
C_L	=	lift coefficient
C_p	=	pressure coefficient
c_f	=	skin-friction coefficient
n	=	coordinate in principal normal direction
s	=	arc length along streamline
$\boldsymbol{u}$	=	velocity vector
x, y, z	=	cartesian coordinates
η	=	distance normal to surface
κ	=	curvature of streamline
κ^n	=	curvature of principal normal
μ	=	dynamic viscosity
$\boldsymbol{\xi}$	=	unit vector along grid line
ρ	=	density

Subscripts

i, j	=	grid indices
min	=	minimum
max	=	maximum
T	=	target
∞	=	freestream

Superscript

n	=	iteration index

Introduction

JUNCTURE flow has captured the attention of many researchers over the past several decades because its adverse effects are present in many practical applications. Juncture flow occurs when the flow on a body interacts with a surface mounted to that body. An example of this type of flow occurs when the flow on the fuselage of an aircraft interacts with the wing.

One of the main features of juncture flows is flow separation. Flow separation occurs when the oncoming boundary layer on the fuselage encounters a steep adverse pressure gradient as the flow approaches the wing. As a result of flow separation, streamwise vorticity is created in the juncture. The streamwise vorticity contained within the horseshoe vortex originates in the upstream boundary layer and is skewed into the streamwise direction during the formation of the vortex. This horseshoe vortex, which wraps around the wing, provides a mechanism for the diversion of low-energy boundary-layer fluid around the wing. This vortex can also reduce the lift and increase the drag of the aircraft. In addition, the regions of concentrated streamwise vorticity that trail behind the juncture decay slowly and interact with components downstream, such as ailerons and engines. Therefore, the horseshoe vortex can also alter the stability and control characteristics of the aircraft.[1]

On aircraft, juncture flow is present at, for example, the wing–fuselage, wing–winglet, wing–pylon, pylon–nacelle, and tail–fuselage junctures. The flow in these junctures can increase the drag, reduce the lift, and adversely affect the stability and control characteristics of the airplane. However, the vortex flow that results from wing leading-edge extensions and fuselage forebodies has been used to improve the performance of airplanes at high angles of attack.[2] In addition to aircraft, juncture flows are present on ships, between the blade and endwall in turbomachinery,[3] at the intersection of a bridge pier and the river bed,[4] in wind-tunnel airfoil testing,[5] and semispan model testing.[6]

Despite the many occurrences of juncture flows, only the flow in the wing–fuselage intersection of aircraft will be considered in this paper. To simplify the configuration, the wing–fuselage intersection was approximated using a wing–plate juncture. However, the design rule developed from this research may be applicable for other juncture flows.

Designing the proper fillet to alleviate one or more of the adverse effects caused by juncture flow can be onerous. For this reason, many researchers have used cut-and-try methods to design fillets to determine whether improvements could be made through filleting.

Kubendran et al.[7] experimentally investigated the laminar flow around an unswept wing of rectangular planform shape with a chord of 6 in. (15.24 cm) and a half-span of 7 in. (17.78 cm). The wing had a NACA 0012 airfoil section. They compared results between the unfilleted wing and two different configurations having fillets with a linear cross section at the leading edge. In both filleted configurations, the section of the wing near the root was linearly stretched so that the maximum thickness of each airfoil section was maintained. The authors were able to eliminate the leading-edge flow separation with these fillets. Although a 9.2% drag reduction was achieved with the larger fillet, a 6.8% increase in drag was obtained with the smaller fillet.

Maughmer[8] tested two leading-edge fillets on a sailplane configuration. One of these fillets had a linear cross section, though it was

Received 29 January 2001; revision received 23 August 2002; accepted for publication 23 August 2002.

*Graduate Research Scholar Assistant, Department of Mechanical and Aerospace Engineering; currently Aerospace Engineer, Naval Air Systems Command, Building 2187 Unit 5 Suite 1320-B, 48110 Shaw Road, Patuxent River, MD 20670. Member AIAA.

†Professor of Engineering and Applied Science, Joint Institute for Advancement of Flight Sciences, Mail Stop 335, Fellow AIAA.

smoothly blended into the wing and fuselage, whereas the other had a parabolic planform. Maughmer claims that a 2–3% drag reduction is possible through filleting. He also declares that the performance of the fillet with a linear planform is better than that of the parabolic fillet planform.

Sung and Lin[9] performed a computational investigation to determine the effects of filleting a wing with a NACA 0020 airfoil section with the nose replaced with a 1.5:1 ellipse. Overall, the authors analyzed five different filleted configurations. Three of the configurations had fillets of linear cross section at the leading edge, whereas two of the configurations had fillets of linear cross section at both the leading and trailing edges. In each of the configurations, the thickness of the incoming boundary layer on the plate was used as the main parameter to determine the size of each of the fillets. The elliptic leading-edge nose section was modified to create the leading-edge fillets, whereas the maximum thickness and shape of the airfoils were maintained aft of the maximum thickness location. Sung and Lin did obtain a small drag reduction with most of their fillets.

As already mentioned, there are many negative aspects of juncture flows. As a result, fillets could be designed to eliminate flow separation, reduce the loss of lift, minimize the drag, or improve the stability and control characteristics. The goal of this research is to develop a method by which a leading-edge fillet can be designed to eliminate flow separation in the wing–plate juncture. Although a reduction in drag is not guaranteed when flow separation is eliminated, any drag reduction obtained would be of great benefit. Though much research has been performed in the area of leading-edge fillet design, a standard design method to eliminate flow separation appears to be absent.

Three-dimensional flow separation occurs when a saddle point is formed on the surface of the body. The saddle point is the location where the shear stress and, hence, the skin friction vanish and the surface streamlines split. Downstream of the saddle point, the surface streamlines begin to converge toward a single streamline, known as the line of separation. Flow separation is eliminated by modifying the skin-friction distribution upstream of the wing leading edge to eliminate the saddle point. Only the flow separation originating upstream of the wing leading edge is considered in this research.

The development of the design rule, which was derived by Green,[10] is briefly discussed in this paper. In addition, the design method that implements the design rule to eliminate flow separation in the wing–fuselage juncture of aircraft is also discussed. The results of two applications of the design method are also presented.

Design Rule

The design rule was developed starting from the three-dimensional incompressible Navier–Stokes equations in streamline coordinates. After taking the derivative of the s-momentum equation, the continuity equation, the s-momentum equation and its derivative were evaluated at the surface. A two-dimensional flow was then assumed and the skin-friction coefficient was written as

$$c_f = \left(\frac{\partial^2 C_p}{\partial s^2} - \kappa^n \frac{\partial C_p}{\partial s}\right) \Bigg/ \left(-\frac{\partial \kappa}{\partial s} + 2\frac{\partial \kappa^n}{\partial n}\right)$$

This equation was then reduced to show that

$$\Delta c_f \propto \Delta \frac{\partial \kappa}{\partial s} \tag{1}$$

Relation (1) predicts the proper trend for a change in skin friction, but is useless for design applications because $\partial\kappa/\partial s$ would be difficult to modify during a design process. To find a parameter more suitable for design, the functional dependence of $\partial\kappa/\partial s$ on the shape of the body was found. A sensitivity study was then performed to show that the largest change in $\partial\kappa/\partial s$ occurs when $\mathrm{d}y/\mathrm{d}x$ is changed. As a result, the relation

$$\Delta c_f \propto \Delta \frac{\mathrm{d}y}{\mathrm{d}x} \tag{2}$$

was obtained. Relation (2) indicates that a change in skin-friction results from a change in the slope of the surface. As a result, the slope of the surface was used in this research to modify the skin-friction distribution to avoid flow separation.

The design rule written in relation (2) was developed assuming a two-dimensional flow. This rule can be applied in three dimensions by making the substitution

$$\frac{\mathrm{d}y}{\mathrm{d}x} = \frac{\mathrm{d}\eta}{\mathrm{d}s}$$

where s is along the streamline and η is normal to the surface. Substituting this equation into relation (2) yields

$$\Delta c_f \propto \Delta \frac{\mathrm{d}\eta}{\mathrm{d}s}$$

Writing the design rule in this form could allow the relationship to be applied in a variety of three-dimensional cases where flow separation occurs, including the design of a corner between two intersecting surfaces.

Approach

Although any Navier–Stokes flow solver could be used to implement the design rule presented in the preceding section, OVERFLOW[11] was chosen as the flow solver for this project. OVERFLOW solves the compressible continuity, Navier–Stokes, and energy equations in strong conservation law form. These equations are solved using finite differences in space and implicit time stepping. Both central differencing and Roe upwind differencing are available within the flow solver. In addition, a block tridiagonal method and a scalar pentadiagonal method are available for implicit time stepping. Moreover, a multigrid method, a low Mach number preconditioning algorithm, and a matrix dissipation algorithm have been included to improve solution convergence and/or quality. For turbulent flow, the Baldwin–Lomax, Baldwin–Barth, Spalart–Allmaras,[12] k–ω, and Menter's shear stress transport turbulence models are available.

In addition, OVERFLOW uses overset grids for complex geometries. This allows the flow solver to be used in a wide variety of applications, including juncture flows.

The Spalart–Allmaras turbulence model[12] was chosen for use with OVERFLOW in the applications presented in this paper. Although this turbulence model was not specifically developed for use in juncture flow problems, it was used with success during the design of standoff geometries for semispan model testing.[6]

The Spalart–Allmaras turbulence model[12] consists of a transport equation for the turbulent viscosity. This model was constructed using empiricism and arguments of dimensional analysis, Galilean invariance, and selective dependence on the molecular viscosity. The model has been used for two- and three-dimensional flows and is compatible with both structured and unstructured grids.

Application of the Design Rule to the Wing–Plate Juncture

The design rule just discussed will now be used to design a leading-edge fillet for a wing–plate juncture.

Strategy for the Implementation of the Design Rule

Relation (2) is used to design a new fillet for the wing. This expression can be rewritten as

$$\Delta\left(\frac{\mathrm{d}z}{\mathrm{d}x}\right)_j = A\Delta(c_f)_j \tag{3}$$

where j is a point on the leading edge of the wing and y has been replaced with z. The coordinate system used for the wing–plate juncture is shown in Fig. 1. In Fig. 1, z is in the spanwise direction.

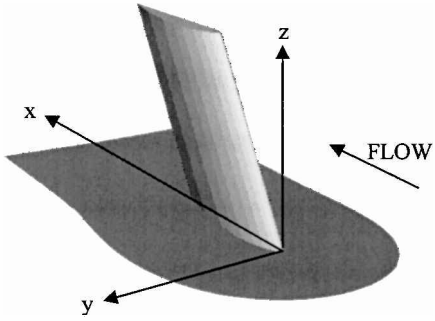

Fig. 1 Coordinate system used for the wing–fuselage juncture.

To apply this equation in the design of a new fillet, both sides are multiplied by $(x_j - x_{j-1})$ to form

$$(x_j - x_{j-1})\Delta\left(\frac{dz}{dx}\right)_j = A\Delta(c_f)_j(x_j - x_{j-1}) \tag{4}$$

Because $(x_j - x_{j-1})$ is independent of the iteration, this term can be distributed through the differential on the left-hand side of Eq. (4) to form

$$\Delta\left[(x_j - x_{j-1})\left(\frac{dz}{dx}\right)_j\right] = A\Delta(c_f)_j(x_j - x_{j-1}) \tag{5}$$

Equation (5) can then be reduced to

$$\Delta(z)_j = A\Delta(c_f)_j(x_j - x_{j-1}) \tag{6}$$

$\Delta(z)_j$ is applied to each point downstream of j so that only the slope at point j is changed. As a result, the new surface of iteration n is given by

$$z_j^n = z_j^{n-1} + A\sum_{i=2}^{j}\left[(c_{f,T})_i - (c_f)_i^{n-1}\right](x_i - x_{i-1}) \tag{7}$$

where the second term on the right-hand side represents the cumulative change made in z at point j and every point upstream. In the case of an unswept wing, the slope at the leading edge of the wing is large because $(x_j - x_{j-1})$ is small. The calculation of the slope is avoided by applying the design rule in the manner shown earlier.

During the design process, Eq. (7) is applied along the grid line containing the leading edge of the wing. Although the design rule was derived from the Navier–Stokes equations in streamline coordinates, Eq. (7) is not applied along a streamline of the flow. It is assumed that the grid line of the leading edge is aligned with a surface streamline.

In Eq. (7), A is chosen to be positive, based on experiments with several design cases. Values of A between 100 and 300 seem to work best.

Design Method

The design process for filleting a wing–plate juncture is shown in Fig. 2. If the initial wing is unfilleted, then a circular fillet is placed on the configuration. In reference to Fig. 1, a circular fillet is a fillet in which the planform shape of the leading edge of the initial wing near the flat plate is extended upstream to create a planform shape that is circular in the x–z plane near the plate. A circular fillet was chosen because it is tangent to both the leading edge of an unswept wing and the flat plate. The radius of the circular fillet is equal to the separation distance ahead of the wing on the unfilleted configuration. The reason for adding this circular fillet is not to eliminate flow separation, but rather to reduce the number of design iterations.

After this new configuration is analyzed, the saddle point on the plate or fillet is located. If a saddle point does not exist, then the grid line along which the preceding saddle point was located is used. Even though the saddle point has been eliminated, it may be

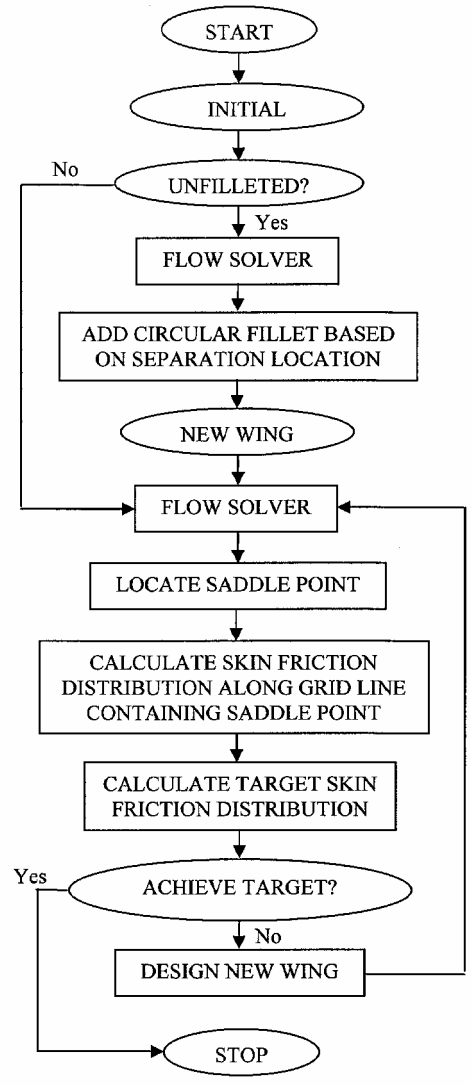

Fig. 2 Flowchart of the design method for wing–fuselage junctures.

desirable to continue iterating the design process, so that the target skin-friction distribution is achieved.

Once the saddle point is located, the skin-friction distribution is calculated along the grid line containing this saddle point. Specifically, the skin-friction distribution in the direction of the grid line is calculated. In other words,

$$c_f = \frac{\mu(\partial/\partial\eta)(\boldsymbol{u}\cdot\boldsymbol{\xi})|_0}{\left(0.5\rho_\infty u_\infty^2\right)}$$

After the skin-friction distribution is calculated, a target skin-friction distribution is determined in two steps. In the first step, a preliminary target skin-friction distribution is calculated as

$$c_{f,T,1} = \max(c_f, c_{f,\min,1}) \tag{8}$$

where c_f is the current skin-friction distribution and $c_{f,\min,1}$ is the minimum allowable skin-friction coefficient. Equation (8) is applied at each point along the grid line containing the saddle point.

In the second step, a constant $c_{f,\min,2}$ is used, where $c_{f,\min,2} \geq c_{f,\min,1}$. The target skin-friction coefficient at a point is

$$c_{f,T} = c_{f,T,1}$$

unless the maximum value of $c_{f,T,1}$ upstream of the current point is greater than $c_{f,\min,2}$ and the maximum value of $c_{f,T,1}$ downstream is greater than $c_{f,\min,2}$, in which case

$$c_{f,T} = c_{f,\min,2}$$

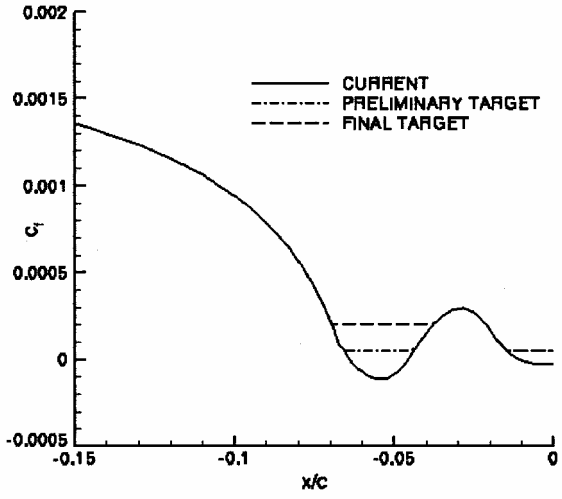

Fig. 3 Sample target skin-friction distribution ahead of the wing leading edge.

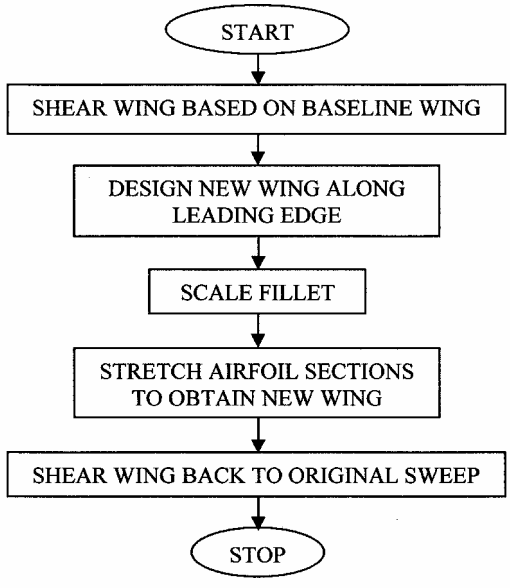

Fig. 4 Flowchart of the design new wing module.

To ensure that the target skin-friction distribution is greater than zero, the value of $c_{f,\min,2}$ is used when a local minimum exists in the skin-friction distribution.

Sample preliminary and final target skin-friction distributions are shown in Fig. 3, where a value of 0.00005 was chosen for $c_{f,\min,1}$, and a value of 0.0002 was chosen for $c_{f,\min,2}$. The final target was determined based on the preceding method. Notice in Fig. 3 that the final target skin-friction coefficient at -5% chord is equal to 0.0002 because the maximum preliminary target skin-friction coefficient both upstream and downstream is greater than 0.00005. At -0.5% chord, on the other hand, the final target skin-friction coefficient is equal to 0.00005 because the maximum skin-friction coefficient downstream is less than 0.00005.

The rationale for choosing a target skin-friction distribution similar to that shown in Fig. 3 is to eliminate the saddle point to eliminate flow separation. Because the skin-friction coefficient vanishes at the saddle point, then the saddle point, and, hence, flow separation will be eliminated by forcing the skin-friction coefficients to be positive.

After calculating the target skin-friction distribution, a new wing is designed in the design new wing module in Fig. 2. The details of this module are shown in Fig. 4.

In the first module in Fig. 4, the wing is sheared as illustrated in Fig. 5. First, a baseline wing must be determined, which will be discussed in more detail later. After the baseline wing is determined,

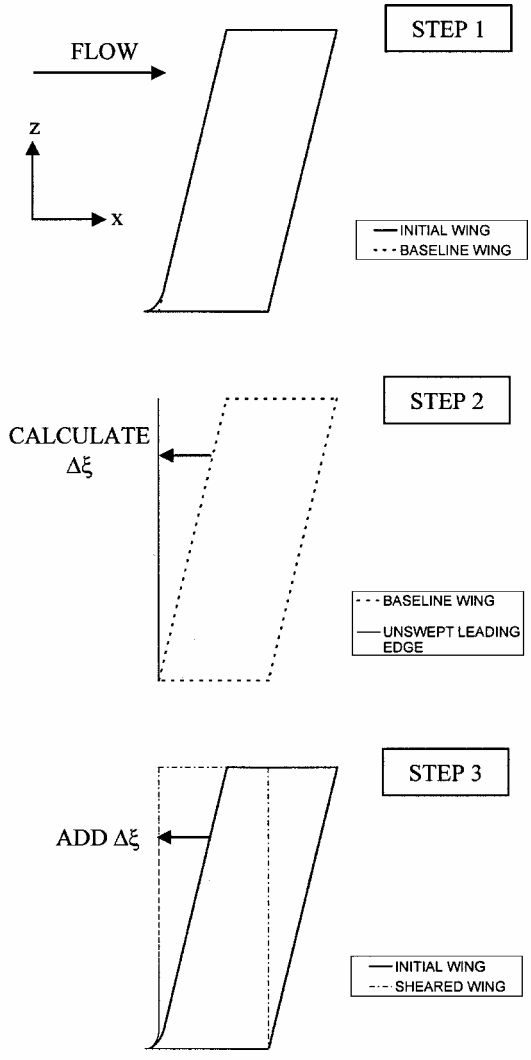

Fig. 5 Process by which a wing is sheared before design.

the function $\Delta\xi$ is calculated, where $\Delta\xi$ varies with z. As shown in Fig. 5, $\Delta\xi$ is the difference in x between an unswept leading edge and the leading edge of the baseline wing. The function $\Delta\xi$ should be negative for baseline wings of positive leading-edge sweep.

In step 3, the sheared wing is obtained by adding the function $\Delta\xi$ to the x ordinates of the initial wing. The sheared wing is the wing to which the design rule will be applied. As a result, there should be no leading-edge sweep on the sheared wing except in the region of the leading-edge fillet.

There are two reasons for shearing the wing. First of all, the size of the leading-edge fillet can easily be scaled in this configuration. Scaling the fillet is important to reducing the size of the leading-edge fillet placed on the wing. Second, shearing the wing allows the new design to be easily blended into the leading edge of the preceding wing, while avoiding any possibilities of having kinks in the leading edge of the new wing.

After shearing the wing, Eq. (7) is used to design a new leading-edge fillet. This equation is applied along the grid line of the leading edge, using the current and target skin-friction coefficients along the line containing the saddle point.

In the next module of Fig. 4, the new fillet is scaled to reduce the height of the leading-edge fillet. If the design method is applied without scaling the leading-edge fillet, then the fillet will become larger than is necessary to eliminate flow separation. When designing a leading-edge fillet for an unswept wing, it was noticed that a local maximum in the skin-friction distribution appeared midway through the design. As the design progressed, the skin-friction coefficient at the local maximum and the size of the leading-edge fillet both grew larger.

The leading-edge fillet is scaled at each point j using the equation

$$z_{j,\text{new}} = \left(z_i^{n-1}/z_i^n\right) z_j^n \tag{9}$$

where i is the location of the local maximum of the current skin-friction distribution and z_j^n is the fillet surface obtained after applying Eq. (7). The value $z_{j,\text{new}}$ becomes the new fillet shape. Notice from Eq. (9) that at point i the value of $z_{i,\text{new}}$ is equal to z_i^{n-1}.

After the fillet is scaled, the next step in Fig. 4 is to stretch the airfoil sections in the fillet region of the current wing to obtain the new wing. Figure 6 illustrates the process by which this is accomplished for a given wing airfoil section. First, the initial airfoil section is divided into its camber distribution and its thickness distribution. Then the camber distribution is linearly extrapolated to align the x ordinate of the leading edge of the camber line with the x ordinate of the new fillet leading edge determined by the method presented earlier. The camber line is extended based on the slope of the camber line at the leading edge of the initial airfoil.

After extending the camber line in Fig. 6, the thickness distribution of the initial airfoil is distributed along the new camber line to obtain the stretched airfoil. The maximum thickness of the airfoil section is maintained while the thickness along the new camber line is distributed. The maximum thickness ratio, however, is reduced because the chord length of the stretched airfoil is larger than that of the initial airfoil. The process for extending the camber line is applied to each airfoil section in the wing.

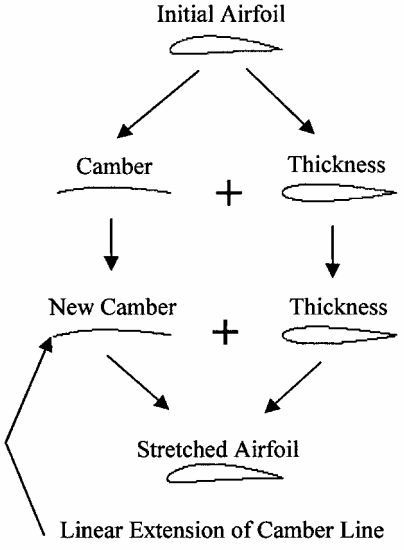

Fig. 6 Process by which the airfoil sections are stretched to obtain the new wing.

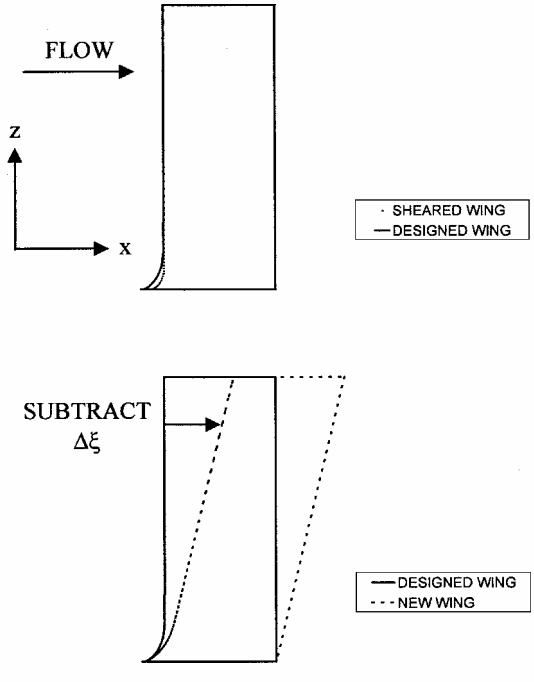

Fig. 7 Process by which a wing is sheared after design.

The next step in Fig. 4 is to shear the wing back to its original sweep. This is demonstrated in Fig. 7, where the function $\Delta\xi$ calculated in Fig. 5 is subtracted from the current unswept wing to obtain the new wing.

After completing the design new wing module in Fig. 2, the process is iterated until flow separation is eliminated.

Results

The design method just presented was used to redesign several unfilleted configurations. These configurations include an unswept wing without lift and a lifting wing with 30-deg sweep. The results of each of the design cases are presented and discussed in the following sections.

Unswept Wing

In this example, an unswept wing without a fillet was redesigned to eliminate flow separation ahead of the wing leading edge. The wing had a rectangular planform shape with unit chord and a half-span of 1.16 chords. The wing had a NACA 0012 airfoil section and was analyzed at a Mach number of 0.2 and a Reynolds number of 1×10^7 at an angle of attack of 0 deg. Because the wing is symmetric and the angle of attack is 0 deg, only one-half of the configuration was analyzed. A grid refinement study was performed to verify that the grid size was adequate to model the flow in the juncture accurately.[10]

The wing was redesigned using the method described earlier. Because the flow and geometry are symmetric, the saddle point is located in the symmetry plane ahead of the wing leading edge. Thus, the skin-friction distribution on the symmetry plane of the plate ahead of the initial wing is shown in Fig. 8. The leading edge of the wing is at $x = 0$. It can be seen in Fig. 8 that the skin-friction coefficient vanishes on the initial wing at approximately 3% chord ahead of the wing leading edge. This indicates that the saddle point is at this location.

Because the initial wing did not have a fillet, a fillet with a circular planform was added to the leading edge of the wing. The radius of the circular fillet is 3% chord, which is equal to the separation distance ahead of the leading edge of the unfilleted wing. The skin-friction distribution associated with this intermediate wing is also shown in Fig. 8. From Fig. 8, one can see that the skin-friction coefficient vanishes near −3.5% chord for the intermediate wing, indicating that flow separation still exists.

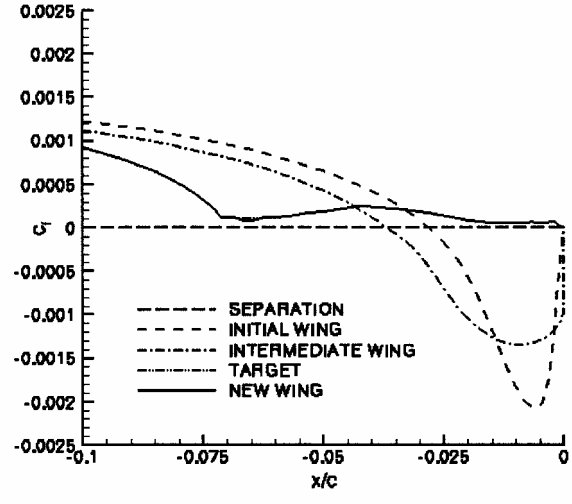

Fig. 8 Skin-friction distribution along the symmetry plane of the plate for the initial and new wing configurations for the case without sweep.

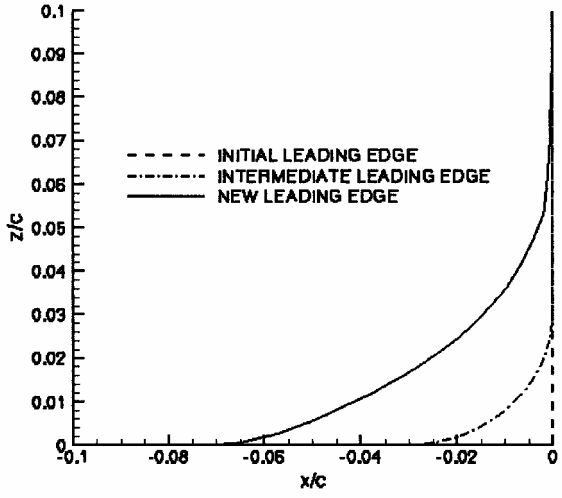

Fig. 9 Fillet shape of the new wing for the case without sweep.

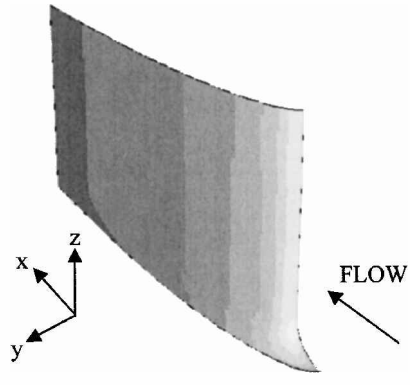

Fig. 10 New wing for the case without sweep.

The target skin-friction distribution and the skin-friction distribution for the new configuration are also shown in Fig. 8. There is excellent agreement between these two curves, indicating that the design method was successful in increasing the skin-friction distribution toward the target distribution. Because the skin friction does not vanish until near the wing leading edge, the flow separation has been eliminated. In determining the target skin-friction distribution in this plot, values of 0.00001 and 0.0001 were used for $c_{f,\min,1}$ and $c_{f,\min,2}$, respectively.

The fillet shape for the initial, intermediate, and new wings are shown in Fig. 9. From Fig. 9, one can see that the fillet for the new wing extends nearly 7% chord ahead of the wing leading edge. Also, the fillet extends to a height of about 7% chord in the z direction. Because many researchers in the past have correlated the required leading-edge fillet size to plate boundary-layer height, note here that the boundary-layer height on the plate at the wing leading edge is about 5% chord. A three-dimensional view of the new wing is shown in Fig. 10.

A comparison of the surface streamlines of the unfilleted wing and the filleted wing is shown in Fig. 11. The surface streamlines are the lines that are tangent to the surface shear stress. In Fig. 11, the surface streamlines are shown from a viewpoint located upstream of the leading edge of the wing, looking into the corner of the leading edge at an angle of about 45 deg to the flat plate. The surface streamlines of the unfilleted configuration are shown on the left-hand side of Fig. 11, whereas the surface streamlines of the new configuration are shown on the right-hand side of Fig. 11. The saddle point on the unfilleted configuration is labeled S in Fig. 11. Notice that this saddle point has been eliminated on the new configuration and flow separation no longer exists.

The drag coefficients of the two configurations are compared in Table 1. Table 1 indicates that the drag remains relatively unchanged, even though flow separation has been eliminated.

Table 1 Comparison of drag coefficients between unfilleted and filleted wings for the case without sweep

Wing	C_D, viscous	C_D, pressure	C_D, total
Unfilleted	0.0072	0.0008	0.0080
Filleted	0.0073	0.0008	0.0081

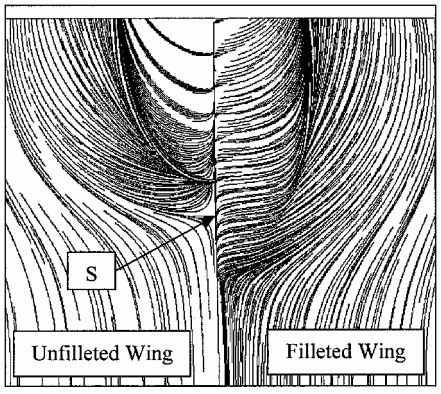

Fig. 11 Comparison between the surface streamlines of the unfilleted and filleted wings for the case without sweep.

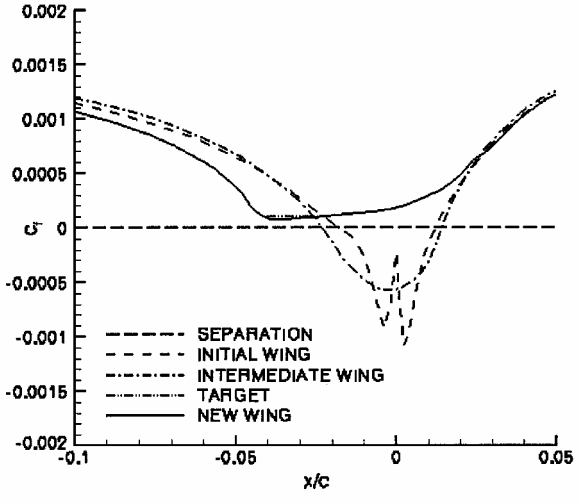

Fig. 12 Skin-friction distribution along the symmetry plane of the plate for the initial and new wing configurations for the case with 30-deg sweep.

A value of 150 was used for parameter A in Eq. (7). This design required 37 iterations and 82 CPU hours on a Silicon Graphics Octane computer with an R12000 processor. The flow solver was run for 100 iterations between each design, ensuring that the skin friction was converged to 0.00001 before the design was complete.

Lifting Wing with 30-Degree Sweep

The design method was also used to redesign a lifting wing with a 30-deg leading-edge sweep. The wing was of constant unit chord and had a half-span of 1.16 chords. The wing had a NACA 4412 airfoil section and was redesigned at a Mach number of 0.2 and a Reynolds number of 1×10^7 at an angle of attack of 0.5 deg.

The skin-friction distribution of the initial wing along the grid line containing the saddle point is shown in Fig. 12. Because the skin-friction coefficient vanishes at about 2% chord ahead of the wing leading edge, flow separation does exist. Because the initial wing was unfilleted, a fillet with a circular planform was added to the wing. The skin-friction distribution for this intermediate wing is also shown in Fig. 12. From Fig. 12, one can see that the skin-friction coefficient vanishes near −2.5% chord, indicating that flow separation still exists.

Table 2 Comparison of lift and drag coefficients between unfilleted and filleted wings for the case with 30-deg sweep

Wing	C_D, viscous	C_D, pressure	C_D, total	C_L
Unfilleted	0.0141	0.0063	0.0204	0.390
Filleted	0.0142	0.0062	0.0204	0.390

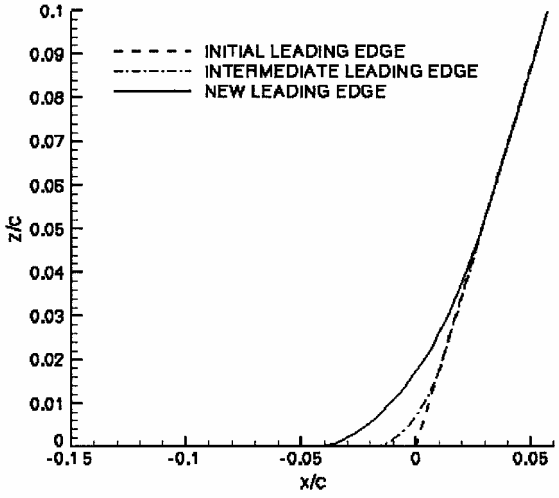

Fig. 13 Fillet shape of the new wing for the case with 30-deg sweep.

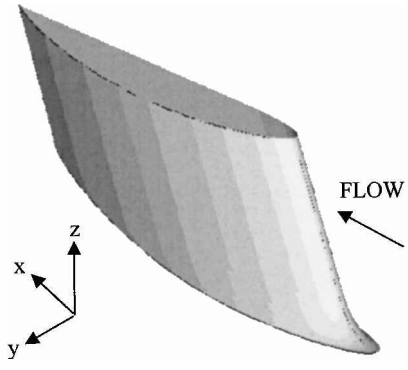

Fig. 14 New wing for the case with 30-deg sweep.

The target skin-friction distribution and the skin-friction distribution of the new wing are also shown in Fig. 12. A value of 0.0001 was used for $c_{f,\min,1}$ and $c_{f,\min,2}$ in determining the target skin-friction distribution. Notice in Fig. 12 that the target skin-friction distribution and the skin-friction distribution of the new wing agree well. This indicates that the design method was successful in eliminating flow separation.

Figure 13 shows the leading-edge shape of the initial, intermediate, and new wings. From Fig. 13, one can see that the leading-edge fillet of the new wing extends to approximately 4% chord upstream of the leading edge and about 5% chord in the z direction. A three-dimensional view of the wing is shown in Fig. 14.

The surface streamlines of the unfilleted and filleted wings are shown in Fig. 15. In Fig. 15, the surface streamlines are shown from a viewpoint located upstream of the leading edge of the wing, looking into the corner of the leading edge at an angle of about 45 deg to the flat plate. In Fig. 15a, the surface streamlines for the unfilleted wing indicate that flow separation exists. The location of the saddle point is indicated with the letter S. In Fig. 15b, the surface streamlines show that both the saddle point and flow separation have been eliminated.

The lift and drag coefficients of the initial wing and new wing are compared in Table 2. Once again, the lift and drag did not change significantly as a result of the elimination of flow separation.

A value of 200 was used for parameter A in Eq. (7). This design required 26 iterations and 115 CPU hours on a Silicon Graphics

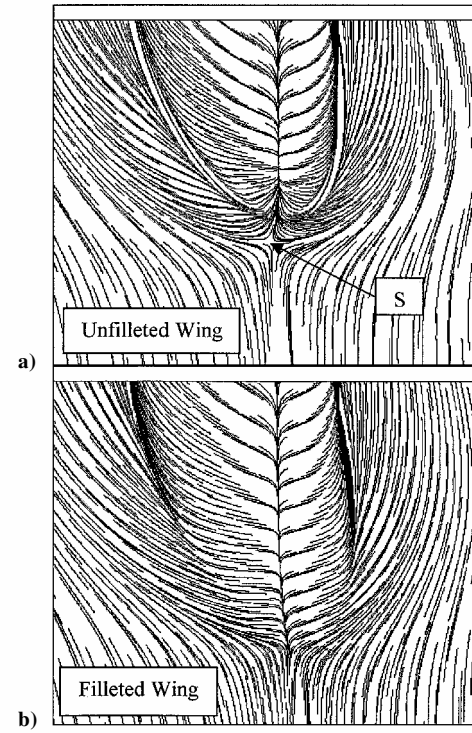

Fig. 15 Comparison between the surface streamlines of the unfilleted and filleted wings for the case with 30-deg sweep.

Octane computer with an R12000 processor. The flow solver was run for 100 iterations between each design. Once again, 100 iterations were adequate to ensure that the skin friction was converged to 0.00001 before the design was complete.

Conclusions

A design method has been developed whereby a leading-edge fillet for a wing can be designed to eliminate flow separation in the wing–fuselage juncture of aircraft. After calculating the current skin-friction distribution ahead of the leading edge of the wing, a target skin-friction distribution is specified that would eliminate flow separation ahead of the wing leading edge. Then, a new design rule, which relates a change in skin friction to a change in the slope of the surface, is used to move the current skin-friction distribution toward the target distribution by extending the leading edge of the wing forward to form a leading-edge fillet. After determining the shape of the new leading-edge fillet, the configuration is analyzed by the flow solver and the design process is iterated until the target skin-friction distribution is achieved. The method was then shown to eliminate flow separation in two wing–plate junctures.

This design method for leading-edge fillets differs from previously existing methods in that this method employs a skin-friction/slope relationship to eliminate flow separation. Previous methods for designing leading-edge fillets are based primarily on trial- and-error approaches.

The design rule that has been developed could be applied to eliminate flow separation in cases other than wing–fuselage junctures. Because the design rule was derived from the governing equations, the relationship between a change in skin friction and a change in slope should be valid in many other cases where flow separation occurs. Some examples of potential applications of the design rule include automobiles, trucks, trains, ships, submarines, torpedoes, and missiles.

References

[1]Visbal, M. R., "Numerical Investigation of Laminar Juncture Flows," AIAA Paper 89-1873, June 1989.

[2]Erickson, G. E., "Wind Tunnel Investigation of Vortex Flows on F/A-18 Configuration at Subsonic through Transonic Speeds," NASA TP-3111, Dec. 1991.

[3]Goldberg, U. C., and Reshotko, E., "Scaling and Modeling of Three-Dimensional, End-Wall, Turbulent Boundary Layers," NASA CR-3792, June 1984.

[4]Zabilansky, L. J., "Ice Force and Scour Instrumentation for the White River, Vermont," Cold Regions Research and Engineering Lab., U.S. Army Corps of Engineers, Special Rept. 96-6, April 1996.

[5]Treaster, A. L., Gurney, G. B., and Jacobs, P. P., "Sidewall Boundary Layer Corrections in Subsonic, Two-Dimensional Airfoil/Hydrofoil Testing," AIAA Paper 84-1366, June 1984.

[6]Milholen, W. E., "A Design Methodology for Semi-Span Model Mounting Geometries," AIAA Paper 98-0758, Jan. 1998.

[7]Kubendran, L. R., Bar-Sever, A., and Harvey, W. D., "Flow Control in a Wing/Fuselage-Type Juncture," AIAA Paper 88-0614, Jan. 1988.

[8]Maughmer, M. D., "An Experimental Investigation of Wing/Fuselage Integration," AIAA Paper 87-2937, Sept. 1987.

[9]Sung, C.-H., and Lin, C.-W., "Numerical Investigation on the Effect of Fairing on the Vortex Flows Around Airfoil/Flat-Plate Junctures," AIAA Paper 88-0615, Jan. 1988.

[10]Green, B. E., "A Viscous Aerodynamic Method for the Design of Leading-Edge Fillets for Wing–Plate Junctures," Ph.D. Dissertation, Dept. of Mechanical and Aerospace Engineering, George Washington Univ., Washington, DC, May 2000.

[11]Jespersen, D., Pulliam, T., and Buning, P., "Recent Enhancements to OVERFLOW," AIAA Paper 97-0644, Jan. 1997.

[12]Spalart, P. R., and Allmaras, S. R., "A One-Equation Turbulence Model for Aerodynamic Flows," AIAA Paper 92-0439, Jan. 1992.